CHEMISTRY OF MATERIALS

Article

pubs.acs.org/cm

Optimal Ambipolar Charge Transport of Thienylenevinylene-Based Polymer Semiconductors by Changes in Conformation for High-Performance Organic Thin Film Transistors and Inverters

Juhwan Kim,[†] Kang-Jun Baeg,[∥] Dongyoon Khim,[†] David T. James,[⊥] Ji-Seon Kim,[⊥] Bogyu Lim,[@] Jin-Mun Yun,[†] Hyung-Gu Jeong,[†] Paul S. K. Amegadze,[§] Yong-Young Noh,*[,§] and Dong-Yu Kim*[,†,‡]

[†]School of Materials Science and Engineering, Gwangju Institute of Science and Technology, 1 Oryong-Dong, Buk-Gu, Gwangju 500-712, Republic of Korea

[‡]Department of Nanobio Materials and Electronics, Gwangju Institute of Science and Technology, 1 Oryong-Dong, Buk-Gu, Gwangju 500-712, Republic of Korea

[§]Department of Energy and Materials Engineering, Dongguk University, 26 Pil-dong, Jung-gu, Seoul 100-715, Republic of Korea

[∥]Nano Carbon Materials Research Group, Korea Electrotechnology Research Institute (KERI), 12 Bulmosan-ro 10beon-gil, Seongsan-gu, Changwon, Gyeongsangnam-do 642-120, Republic of Korea

[⊥]Department of Physics and Centre for Plastic Electronics, Imperial College London, London SW7 2AZ, U.K.

[@]Department of Materials Science and Engineering, Stanford University, Stanford, California 94305, United States

Supporting Information

ABSTRACT: We report the synthesis and characterization of thienylenevinylene-based donor−acceptor alternating copolymers (PTVPhI-Eh and PTVPhI-C12) as highly efficient ambipolar semiconductors in a thin film transistor. These polymers exhibit significantly improved hole and electron mobilities after thermal annealing. To determine the relationship between ambipolar charge transport and thermal annealing, we investigated these polymers using various analyses such as optical spectroscopy, Raman spectroscopy, computational quantum chemical calculation, X-ray diffraction, atomic force microscopy, and ambipolar charge mobility measurements. In pristine films, the polymer chains exhibited weak intra- and interchain ordering. However, when samples were annealed at sufficiently high temperatures, they exhibited a more ordered intra- and interchain conformation. As a result, we found a strong relationship between intra- and interchain conformational changes of the polymers and corresponding ambipolar charge transport properties during thermal annealing processes. Finally, we demonstrate complementary-like ambipolar inverters using a PTVPhI-Eh polymer. The largely shifted inverting voltage was improved for the thermally annealed inverters, which exhibited large voltage gains (~40).

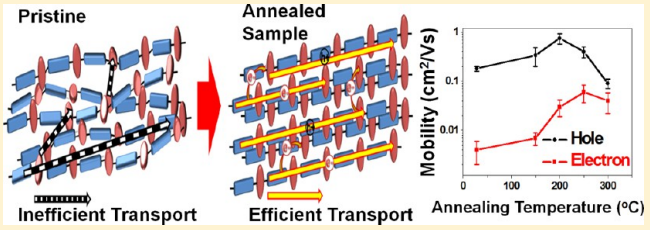

KEYWORDS: *ambipolar polymer, charge transport, OTFTs, thienylenevinylene, polymer conformation*

1. INTRODUCTION

Organic thin film transistors (OTFTs) based on conjugated polymers have attracted much attention in recent years for application as an active layer, because of solution processability and an excellent compatibility with flexible substrates.[1] These unique properties make them useful in the fabrication of various flexible electronics, such as organic integrated circuits (ICs), radiofrequency identification (RFID) tags, and sensors, and memory using cost-effective graphic art printing processes.[2] Because of advances gained over the past two decades, state-of-the-art printed OTFTs boast a charge carrier mobility that is equal to or even higher than that of amorphous silicon TFTs in an active matrix TFT-LCD.[3] To maximize their advantage in the manufacturing process, OTFTs and their circuitry should be fabricated by a process that is as simple as possible. Ambipolarity in charge transport allows the realization of organic CMOS (complementary metal−oxide−semiconductor) ICs via a simple blanket coating without the need for sophisticated micropatterning processes of n- and p-channel conjugated polymers. Therefore, many research groups are actively developing ambipolar conjugated polymers to achieve organic and flexible ICs via a simple large area blanket coating.[4] To realize high-performance ambipolar OTFTs and organic CMOS-based ICs, ambipolar conjugated polymers must meet the following requirements: a high field effect mobility, a low operating voltage, balanced p- and n-channel device characteristics, and a suitable energy level for efficient hole and electron injection from a single electrode, which is typically Au.

Received: December 5, 2012
Revised: March 12, 2013

dx.doi.org/10.1021/cm303908f | *Chem. Mater.* XXXX, XXX, XXX−XXX

Recently, conjugated polymers with alternative donor−acceptor (D−A) moieties in the backbone have been developed for high-performance organic photovoltaics because of the electron push−pull structure that can be used to make low-band gap polymers and the ability to control the copolymer highest occupied molecular orbital (HOMO) and lowest unoccupied molecular orbital (LUMO) energies independently.[5] In addition, D−A polymers can also enhance the intermolecular interaction leading to a small $\pi-\pi$ stacking distance caused by the dipole interaction between donor and acceptor moieties. Therefore, D−A polymers are expected to be a new alternative for active materials in OTFTs with efficient electron and hole ambipolar transport. However, most of the existing polymers predominantly exhibit unipolar (p- or n-type) transport behavior or lower-level and unbalanced ambipolar transport. Among them, excellent ambipolar transport characteristics have been reported for some D−A polymers containing diketopyrrolopyrrole (DPP), rylene imide, and benzobisthiadiazole (BBT) as electron deficient units.[4,6] McCulloch and co-workers have reported the synthesis of DPP and a thieno[3,2-*b*]thiophene-based copolymer (PDPP-TT-T-TT), with hole and electron mobilities of 1.42 and 0.063 $cm^2\ V^{-1}\ s^{-1}$, respectively.[5d] Naphthalenebiscarboximide-bithiophene copolymer (PNIBT) with ambipolar mobilities of 0.003 $cm^2\ V^{-1}\ s^{-1}$ for holes and 0.04 $cm^2\ V^{-1}\ s^{-1}$ for electrons and a high gain of 30 from a PNIBT-based ambipolar inverter was synthesized by Jenekhe and co-workers.[4c] Wudl and co-workers also synthesized a BBT-based copolymer, in which BBT was paired with dithienopyrrole, dithienocyclopentane, dithienosilole, and fluorene. In these copolymers, a BBT-dithienocyclopentane-paired copolymer showed evenly balanced ambipolar properties, with hole and electron mobilities of 0.13 and 0.1 $cm^2\ V^{-1}\ s^{-1}$, respectively.[4d] Herein, these previous results imply the design approach for the achievement of excellent ambipolar polymers, and consequently, the following design requirements are suggested: (i) a structural highly planar π-conjugated unit for efficient hole and electron transport by efficient π-orbital delocalization, largely delocalized LUMO and HOMO orbitals, and solid-state packing such as favorable intermolecular $\pi-\pi$ stacking; (ii) a decrease in LUMO energies by using an electron deficient unit or an electron-withdrawing substituent to enhance electron transport and air stability; (iii) alkyl side chains for solubility and processability with little or no steric hindrance to the backbone. To satisfy those design requirements, D−A-type conjugated polymers with fused aromatic donor and acceptor moieties are ideal structures because the fused structures allow highly planar conformations and strong $\pi-\pi$ interactions. Regrettably, it is relatively difficult to synthesize fused aromatic compounds. In addition, the solubility of such planar fused polymer systems decreases as the size of the fused ring increases. Therefore, donor and acceptor moieties that can be facilely synthesized and satisfy the design requirements mentioned above are needed for successful achievement of excellent ambipolar polymers.

Material design and control of processing conditions are important factors in obtaining well-balanced charge transport properties in ambipolar conjugated polymers. Many previous reports suggest several approaches to the process of improving ambipolar properties such as high-temperature annealing and charge injection engineering via chemical modification of the electrode or the insertion of an interlayer between an organic active layer and an electrode, to control electron and hole mobility.[7] Despite many related studies of ambipolar conjugated polymers, it is not yet fully understood how the process of controlling ambipolar transport affects device performance. Therefore, the study of ambipolar transport through new polymers is needed to gain insight into the mechanisms of charge transport in ambipolar conjugated polymers.

In this study, we synthesized and characterized ambipolar D−A polymers using a new combination of a donor and an acceptor based on the aforementioned design requirements. First, a thienylenevinylene (TV) unit was introduced as an electron-donating building block. The TV unit has good planarity and an extended π-conjugation because of the presence of a vinylene spacer between the thiophene units. This was expected to induce a high hole mobility and a low band gap in the polymer.[8] Also, sufficient solubility was induced as a result of alkyl substitution at position 3 or 4 or at both positions of the thiophene in the TV unit. Our previous work demonstrated the potential of an alkyl-substituted TV building block that showed a high crystallinity and mobility as well as excellent solubility.[3a] An imide-functionalized π-system, as an electron deficient unit, was also introduced to complete the D−A polymer. Electron deficient imide-functionalized π-systems are gaining attention as a new approach to high-mobility n-type or ambipolar materials, because of their planar structure and the strong intermolecular interactions among the imide groups.[9] Imide-functionalized π-systems with these properties have been employed to impart strong electron transport characteristics and also to alter the band gap when inserted into polythiophene backbones. Among these imide-functionalized moieties, *N*-alkyl-3,6-dibromophthalimides are a sufficiently promising electron-accepting unit for the D−A copolymer.[10] These moieties are very useful versatile building blocks because their synthesis involves only two facile steps and because varied alkyl substitution can be conducted on the imide nitrogen atom to control the solubility, packing, and morphology. In addition, it is well-known that phthalimides improve air stability and reliability because they lead to a decrease in HOMO levels via the electron withdrawing nature of an imide.[11] Therefore, we chose phthalimide as the accepting unit in a D−A polymer for this study. The dodecyl-substituted TV and phthalimide-paired copolymers (PTVPhI-Eh and PTVPhI-C12) exhibited lower HOMO levels (−5.24 eV) and good ambipolar transport characteristics.

Here, we describe the intra- and interchain conformational changes of this ambipolar D−A polymer, PTVPhI polymers, under various annealing conditions using optical spectroscopy, Raman spectroscopy, computational quantum chemical calculation, X-ray diffraction (XRD), and atomic force microscopy (AFM). OTFTs based on these polymers exhibited further increased electron and hole mobilities via the annealing process, which also resulted in balanced ambipolar mobility. We found a relationship between ambipolar charge transport and intra- and interchain conformational changes upon thermal annealing of PTVPhI polymers. According to the results of this study, the hole and electron mobilities of these polymers are affected by a combination of intra- and interchain conformational changes. In particular, electron mobility is more significantly affected by interchain conformational changes than by changes of hole mobility. Finally, complementary ambipolar inverters were demonstrated by spin-coating without patterning, resulting in a sharp switching signal and large voltage gains (~40). In addition, a large shift in inverting voltage in pristine OTFTs was greatly improved for the thermally annealed devices

dx.doi.org/10.1021/cm303908f | *Chem. Mater.* XXXX, XXX, XXX−XXX

because of the achievement of a more balanced hole and electron mobility.

2. EXPERIMENTAL SECTION

Materials. All chemicals were purchased from Aldrich and used without further purification. 3-Dodecylthiophene, 2-bromo-3-dodecylthiophene, 3-dodecylthiophene-2-carboaldehyde, (*E*)-1,2-(3,3′-didodecyl-2,2′-dithienyl)ethylene, 5,5′-ditrimethylstannyl-(*E*)-1,2-(3,3′-didodecyl-2,2′-dithienyl)ethylene, 3,6-dibromophthalic anhydride, and *N*-alkyl-3,6-dibromophthalimide were synthesized as reported previously.[3a,10] All reactions were conducted in a nitrogen atmosphere using commercial solvents, unless otherwise stated. ^{1}H NMR spectra were recorded on a JEOL JNM-ECX400, 400 MHz spectrometer in $CDCl_3$. Chemical shifts are reported as parts per million relative to an internal TMS standard. Elemental analysis was recorded on an EA1112 instrument (CE Instrument). The number-average molecular weight (M_n) and weight-average molecular weight (M_w) were determined using gel permeation chromatography (GPC) (YOUNGLIN Acme 9000 instrument) with chloroform as the eluent (flow rate of 1 mL/min, at 35 °C) and were calibrated using a narrow polydispersity polystyrene as the standard.

5,5′-Ditrimethylstannyl-(*E*)-1,2-(3,3′-didodecyl-2,2′-dithienyl)ethylene (1). ^{1}H NMR (400 MHz, $CDCl_3$): δ 6.99 (s, 2H), 6.92 (s, 2H), 2.65 (t, 4H), 1.61 (m, 4H), 1.33 (br, 36H), 0.88 (t, 6H), 0.36 (s, 18H). Anal. Calcd (%): C, 56.22; H, 8.49; S, 7.50. Found (%): C, 56.37; H, 8.43; S, 7.53.

***N*-(2-Ethylhexyl)-3,6-dibromophthalimide (2a).** ^{1}H NMR (400 MHz, $CDCl_3$): δ 7.63 (s, 2H), 3.56 (d, 2H), 1.80 (m, 1H), 1.29 (m, 8H), 0.88 (m, 6H).

***N*-Dodecyl-3,6-dibromophthalimide (2b).** ^{1}H NMR (400 MHz, $CDCl_3$): δ 7.62 (s, 2H), 3.66 (t, 2H), 1.65 (m, 2H), 1.27 (m, 18H), 0.85 (t, 3H).

Polymerization Procedure. Compound **1** (0.5 mmol) and compound **2** (0.5 mmol) were dissolved in anhydrous chlorobenzene and purged with nitrogen. The catalyst, $Pd_2(dba)_3$ (0.01 mmol), and the ligand, P(*o*-tolyl)$_3$ (0.08 mmol), were added to the resultant mixture, and the mixture was refluxed at a constant temperature of 120 °C for 48 h. Subsequently, the resultant reaction mixture was cooled to room temperature and precipitated from a solution in which 150 mL of MeOH was mixed with 30 mL of HCl. The precipitate was filtered to obtain the desired polymers. The final polymers were purified by multiple Soxhlet extractions and vacuum drying.

PTVPhI-Eh. ^{1}H NMR (400 MHz, $CDCl_3$): δ 7.79 (s, 2H), 7.71 (s, 2H), 7.12 (s, 2H), 3.62 (br, 2H), 2.75 (br, 4H), 1.89 (br, 1H), 1.69 (br, 4H), 1.25 (m, 44H), 0.86 (m, 12H). Anal. Calcd (%): C, 76.38; H, 9.61; N, 1.78; S, 8.16. Found (%): C, 75.89; H, 9.38; N, 1.66; S, 7.98.

PTVPhI-C12. ^{1}H NMR (400 MHz, $CDCl_3$): δ 7.79 (br, 2H), 7.73 (s, 2H), 7.12 (s, 2H), 3.70 (br, 2H), 2.75 (br, 4H), 1.70−1.25 (br, 60H), 0.86 (m, 9H). Anal. Calcd (%): C, 76.99; H, 9.93; N, 1.66; S, 7.61. Found (%): C, 76.38; H, 9.77; N, 1.53; S, 7.80.

Characterization. Thermogravimetric analyses (TGA) were conducted with a TA-2050 instrument at a heating rate of 10 °C/min in a nitrogen atmosphere. Differential scanning calorimetry (DSC) analyses were performed on a TA2010 instrument at a heating rate of 10 °C/min in a nitrogen atmosphere. UV−vis spectra were measured using a Perkin-Elmer Lambada 750 instrument. Cyclic voltammetry measurements of the polymers were performed using an AUTOLAB Eco Chemie instrument at a scan rate of 50 mV/s. The sample of polymers was measured using indium tin oxide (ITO) as the working electrode, a Pt wire as the counter electrode, and a Ag wire as the reference electrode in an acetonitrile solution with 0.1 M tetrabutylammonium perchlorate (Bu_4NClO_4) as the supporting electrolyte. XRD data of polymer thin films were recorded under room-temperature conditions using a Rigaku RINT 2000 diffractometer with Cu Kα radiation. AFM data were measured using a Digital Instruments multimode atomic force microscope.

Raman Measurements. Raman spectra were recorded using a Renishaw inVia Raman microscope with a 785 nm laser diode excitation source. A 50× objective was used to focus the laser spot onto the sample for an exposure time of 1 s with five accumulations, which resulted in a good signal-to-noise ratio with little or no background fluorescence signal. All samples were measured in air and required no special sample preparation.

Quantum Chemical Calculations. To interpret the Raman spectra, quantum chemical calculations were performed on the PTVPhI monomer in the virtual gas phase using GAUSSIAN09. To save on computation cost without significantly altering the results of the calculated properties, the long alkyl side chains were replaced with methyl groups.[12] Molecules were first structurally optimized followed by vibrational frequency calculation using density functional theory (DFT) at the B3LYP level of theory[13] and using the 6-31G* basis set. To evaluate the dependence of the vibrational modes on backbone planarity, the thienylenevinylene-phthalimide dihedral angle was frozen in a range of values, and the structure was reoptimized before calculation of the vibrational frequencies of the twisted structures. An empirical scaling factor of 0.96 was applied to the calculated wavenumbers for comparison with the experimental spectra.[14] Molecular orbital distributions along the conjugated backbone were calculated by first structurally optimizing a PTVPhI dimer and trimer in the gas phase using the Austin Model 1 (AM1) semiempirical method. Excited-state energy calculations were then performed on the optimized structures using Zerner's Intermediate Neglect of Differential Orbital method (ZINDO/S), from which the HOMO and LUMO isosurfaces were mapped.[15]

Fabrication and Characterization of OTFTs and Inverters. OTFTs and inverters were fabricated on Corning Eagle 2000 glass substrates with evaporation of gold/nickel (Au/Ni) (15/3 nm) patterns (Ni was the adhesion layer) for the S/D electrodes [channel width (W) = 1 mm, channel length = 20 μm, $W_n/L_n = W_p/L_p$] using a conventional lift-off photolithography technique. The conjugated polymers, PTVPhI-Eh and PTVPhI-C12, were dissolved in anhydrous chlorobenzene to yield 10 mg/mL solutions. The conjugated polymer solutions were spin-coated onto the as-cleaned substrates. The polymer films were thermally annealed at 150, 200, 250, and 300 °C for 30 min, in a nitrogen glovebox. For the polymer gate dielectric layers, PMMA (Aldrich, molecular mass of 120 kDa) was used without further purification. PMMA (80 mg/mL) was dissolved in *n*-butylacetate and filtered with a 0.2 μm PTFE syringe filter before spin-coating. The PMMA dielectric layer had a thickness of ∼520 nm, as measured by an XP-1 Surface profiler system (Ambios Technology). After the dielectric coating, the devices were finally annealed at 80 °C for 2 h in the same glovebox. The top-gate transistors were completed by forming gate electrodes on the active regions of the transistors via the evaporation of thin Al films (∼30 nm) with a metal shadow mask. The electrical characteristics of the fabricated individual polymer TFTs and the static characteristics of the complementary inverter circuits were measured using a Keithley 4200-SCS instrument in a glovebox under a nitrogen atmosphere.

3. RESULTS AND DISCUSSION

Synthesis and Characterization of Polymers. To establish synthetic motivation, we simulated the repeating unit of PTVPhI polymers using the B3LYP density functional theory method. This simulation result shows the planar conformation of the PTVPhI repeating unit, as shown in Figure 1. This can be attributed to the strong planarizing effect of the vinylene linker. Also, the planar conformation of the PTVPhI repeating unit shows that the conformation of the molecule matched well with our synthetic intention.

Both polymers (PTVPhI-Eh and PTVPhI-C12) were synthesized via a Stille coupling polymerization between 5,5′-ditrimethylstannyl-(*E*)-1,2-(3,3′-didodecyl-2,2′-dithienyl)-ethylene and *N*-alkyl-3,6-dibromophthalimide using $Pd_2(dba)_3$/P(*o*-tolyl)$_3$ in chlorobenzene via the synthetic route shown in Scheme 1. Sufficient solubility of both polymers was achieved by attaching branched 2-ethylhexyl and a sufficiently long *n*-dodecyl chain. These polymers showed high solubility in

dx.doi.org/10.1021/cm303908f | Chem. Mater. XXXX, XXX, XXX−XXX

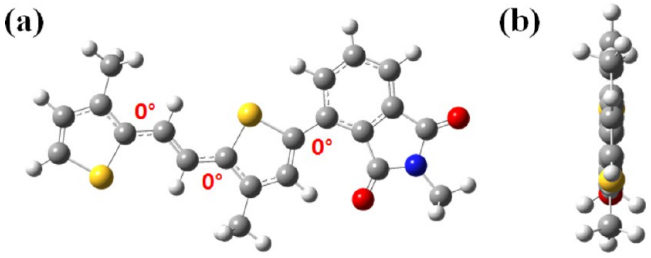

Figure 1. Structural simulation of a PTVPhI backbone: (a) front view and (b) side view.

common organic solvents such as chloroform (~30 mg/mL), tetrahydrofuran (~20 mg/mL), and chlorobenzene (~30 mg/mL) because of the presence of sufficient alkyl side chains consisting of TV and phthalimide units. The final copolymers had number-average molecular weights (M_n) of 18600 g/mol (PTVPhI-Eh) and 17800 g/mol (PTVPhI-C12), as determined by GPC versus a polystyrene standard. The thermal properties of the polymers were measured by TGA and DSC, as shown in Figure S1 of the Supporting Information. The TGA thermograms of PTVPhI-Eh and PTVPhI-C12 revealed high decomposition temperatures (5% weight loss) of 414 and 399 °C, respectively, under a nitrogen atmosphere, which indicated good thermal stability because of the presence of a phthalimide group. Interestingly, PTVPhI-Eh with a branched ethylhexyl side chain showed a meltinglike thermal transition, while common polymers with the branched side chain do not exhibit such thermal transitions due to either poor molecular ordering or the amorphous nature of the bulky chains.[16] PTVPhI-Eh and PTVPhI-C12 showed meltinglike thermal transitions (T_m) at 260 and 293 °C, respectively. This means that PTVPhI-Eh can conduct chain motion or reorganization at a temperature that is relatively lower than that for PTVPhI-C12. The HOMO energetic levels for both polymers were measured using cyclic voltammetry. The HOMO levels of PTVPhI-Eh and PTVPhI-C12 were determined to be −5.24 and −5.18 eV, respectively, as shown in Figure S2 of the Supporting Information. The LUMO level was estimated using the optical band gap (~1.83 eV) and HOMO levels. The LUMO levels of PTVPhI-Eh and PTVPhI-C12 were calculated as −3.39 and −3.33 eV, respectively. These results are summarized in Table 1.

Optical Properties of Polymers. The UV−vis absorption spectra of both polymers were measured to establish the effect of thermal annealing on the optical properties. The absorption spectra of both polymer films showed a red shift of ~44 nm compared with those in solution. This red shift is caused by strong interchain interaction between the polymeric chains in the thin film. As shown in Figure 2a, the absorption spectra of the PTVPhI-Eh film showed significant changes after thermal annealing. For the pristine film, the absorption spectrum showed two peaks at 568 and 620 nm. After annealing had been conducted from 150 to 200 °C, the spectra showed red shifts and increased absorption intensities. The film annealed at 250 °C exhibited further increased absorption. It was noted that strong reorganization of the polymer chains upon thermal annealing had induced a red shift and an increased absorption intensity of the annealed samples, either from strong interchain contact or from an increased level of molecular ordering of the conjugated backbone, i.e., either a polymer packing arrangement or a polymer backbone planarity. With further increases in the annealing or heating temperature from 250 to 300 °C, the absorption spectra of PTVPhI-Eh films showed a blue shift of absorption onset and a drastic diminution in intensity, indicating a change in the conformation or intermolecular aggregations. Similarly, PTVPhI-C12 films showed a red shift and increased absorption intensity from pristine to 250 °C, as shown in panels b and d of Figure 2. In addition, heating (annealing above T_m) the film at 300 °C showed a blue shift and a decrease in absorption. To obtain more detailed information about the structural conformation of both

Scheme 1. Synthetic Routes to Alkyl-Substituted TV-Based Copolymers[a]

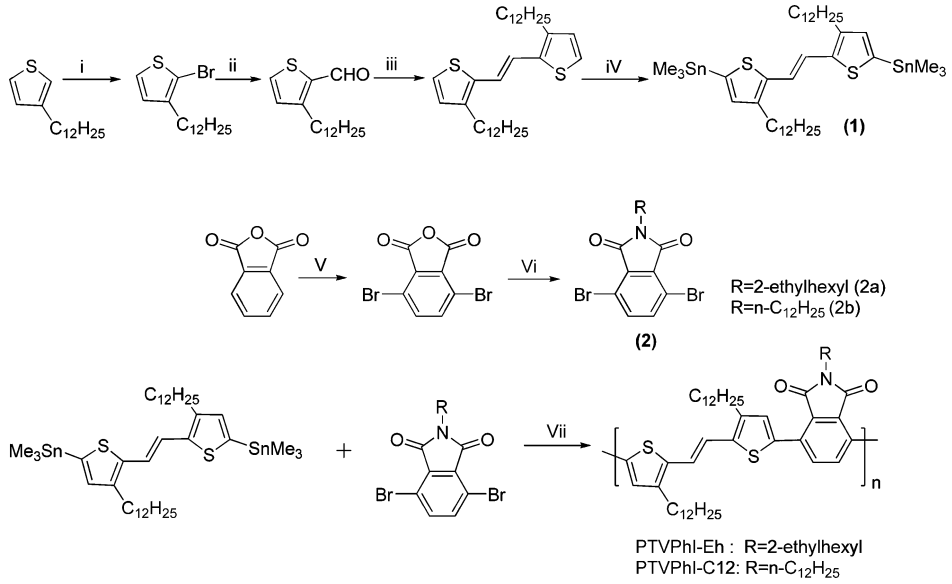

[a]Reagents and conditions: (i) NBS, CH_3Cl/AcOH, 0 °C; (ii) Mg, DMF, THF, reflux; (iii) $TiCl_4$, Zn, pyridine, THF, 0 °C to reflux; (iv) *n*-BuLi, Me_3SnCl, THF, −78 °C to room temperature; (v) bromine, iodine, oleum, 60 °C; (vi) R-amine, AcOH, reflux; (vii) $Pd_2(dba)_3$, chlorobenzene, 120 °C.

dx.doi.org/10.1021/cm303908f | *Chem. Mater.* XXXX, XXX, XXX−XXX

Table 1. Properties of PTVPhI-Eh and PTVPhI-C12

polymer	M_n/M_w[a] (g/mol)	T_d (°C)	T_m (°C)	HOMO[b] (eV)	LUMO[c] (eV)	E_g^{opt}[d] (eV)
PTVPhI-Eh	18600/35800	414	260	−5.24	−3.39	1.85
PTVPhI-C12	17800/35800	399	293	−5.18	−3.33	1.85

[a]Determined by gel permeation chromatography vs a polystyrene standard. [b]Electrochemically determined vs Fc/Fc^+, where ferrocene $E_{1/2}$ = 0.45 V, PTVPhI-Eh E_{onset} = 0.89 V, and PTVPhI-C12 E_{onset} = 0.83 V. [c]$E_{LUMO} = E_{HOMO} + E_g^{opt}$. [d]Optical band gap estimated from the absorption edge of the thin film.

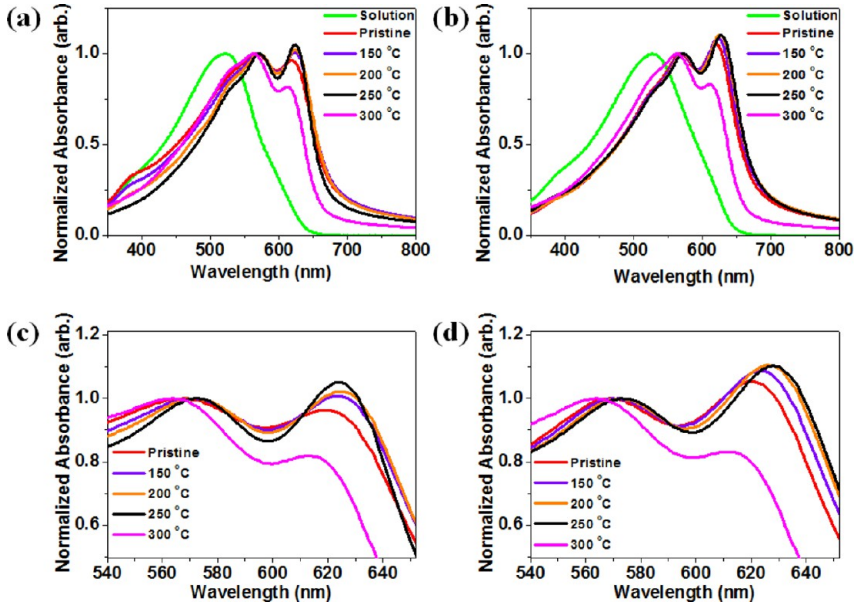

Figure 2. UV−vis absorption spectra of PTVPhI-Eh (a and c) and PTVPhI-C12 (b and d) annealed at various temperatures. Panels c and d show enlarged views of panel a and b, respectively.

polymers following thermal annealing, we measured the Raman spectra and X-ray diffraction of a thin film at various thermal annealing temperatures.

Raman Spectra of Polymer Films. The initial Raman spectra were obtained from solutions of PTVPhI-Eh and PTVPhI-C12 in *p*-xylene to determine the nature of the Raman peaks using calculated vibrational spectra. Previous work has shown that the backbone conformation of conjugated systems in the gas phase is insensitive to large alkyl groups while adding greatly to the computational cost. Therefore, the Eh and C12 alkyl chains were substituted with methyl groups in all calculations to optimize computation time.[12] Both molecules in a *p*-xylene solution exhibited almost identical Raman spectra, supporting the idea that the conjugated cores of isolated molecules are insensitive to long flexible alkyl groups. Prominent Raman peaks at 1418 and 1594 cm^{-1} were observed. The DFT-calculated methyl-substituted monomer showed good agreement with the solution Raman spectra of both PTVPhI-Eh and PTVPhI-C12, suggesting the gas-phase monomer approximation was appropriate in this case. By comparison of the experimental and calculated spectra, the two main Raman modes were identified as belonging to the thiophene (1418 cm^{-1}) and vinyl (1594 cm^{-1}) C═C stretch mode vibrations (Figure 3). For the PTVPhI-Eh polymer in a pristine thin film, both the thiophene and vinyl peaks shifted to lower wavenumbers (from 1418 to 1414.5 cm^{-1} and from 1593.5 to 1592 cm^{-1}, respectively) relative to those of the solution spectrum. Annealing the film at 110 °C further shifted the thiophene peak to a slightly lower wavenumber, while the vinyl mode remained stable. Heating (annealing above T_m) the film at 300 °C had no further effect on the thiophene mode, while the vinyl mode shifted to a slightly higher wavenumber at 300 °C. In the PTVPhI-C12 pristine film, both the thiophene and vinyl modes shifted to a lower wavenumber relative to that of the solution spectrum, with a trend (although a weaker effect) similar to that of the PTVPhI-Eh films. Unlike that of PTVPhI-Eh, further annealing caused a monotonic shift of the PTVPhI-C12 thiophene and vinyl modes to progressively lower wavenumbers.

Interpretation of the Raman Spectra. To explore the significance of the shift in thiophene and vinyl Raman modes, the vibrational spectra of a PTVPhI-methyl monomer with varying torsion angles (40° to 0° in steps of 10°) were calculated (Figure 3e,f). This had the effect of modulating the degree of HOMO−LUMO delocalization along the backbone, with the more planar structure having enhanced conjugation relative to that of the more twisted structure. The results showed unequivocally that for both the thiophene and vinyl modes, the shift to a lower wavenumber signified an increase in the planarity or degree of conjugation along the backbone. Similar results for conjugated systems have been reported previously.[17] Using this analysis, it was possible to determine that for PTVPhI-Eh the level of conjugation in pristine film was greater than it was for PTVPhI-C12 (greater peak shift in PTVPhI-Eh from solution to pristine film), which would suggest better charge transport properties in the PTVPhI-Eh pristine film compared to that in PTVPhI-C12. On subsequent annealing, the PTVPhI-Eh film showed little change in delocalization (small peak shifts) except at 300 °C, where there was a small but noticeable decrease in the level of

dx.doi.org/10.1021/cm303908f | *Chem. Mater.* XXXX, XXX, XXX−XXX

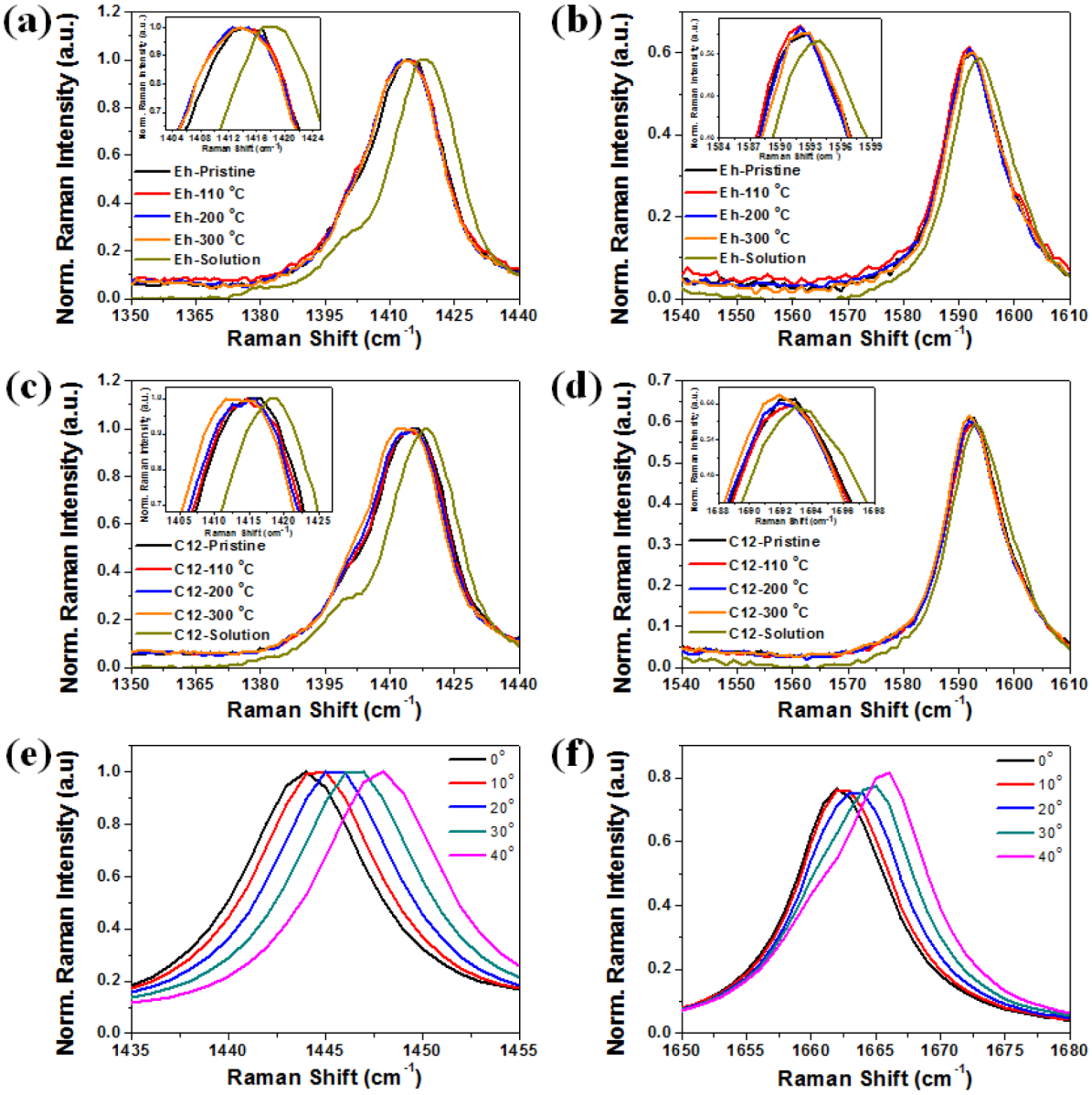

Figure 3. Experimental Raman spectra of the (a) thiophene C═C and (b) vinyl C═C stretch mode for PTVPhI-Eh and (c) thiophene C═C and (d) vinyl C═C stretch mode for PTVPhI-C12 under 785 nm excitation. Enlarged spectra are shown in the insets. Calculated Raman spectra of the (e) thiophene C═C and (f) vinyl C═C stretch mode in the PTVPhI backbone.

conjugation (peak shift to a higher wavenumber). In the PTVPhI-C12 pristine film, despite the fact that the Raman spectrum suggested a smaller increase in the level of conjugation from solution relative to pristine PTVPhI-Eh, further heating (annealing above T_m) to 300 °C showed continually improving conjugation (indicated by the continual peak shifts to lower wavenumbers) with no evidence of a diminished level of conjugation (peak shift to higher wavenumbers) even at 300 °C.

Characterization of OTFTs. Top-gate/bottom-contact (TG/BC) OTFTs were fabricated by spin-coating the PTVPhI-Eh and PTVPhI-C12 solutions in chlorobenzene as the active layer. Both devices showed typical ambipolar OTFT characteristics, such as diodelike current−voltage characteristics in the V-shaped transfer curve (Figure 4). The hole mobility and electron mobility were calculated from the respective saturation regime of the transfer curves using the standard saturation regime equation of metal oxide field effect transistors: $I_{ds} = (\mu WC_o/2L)(V_g - V_t)^2$.[18] Both polymers exhibited a hole and electron mobility change as the annealing temperature was increased as shown in Table 2. When the samples were annealed at 200 °C, the electron mobility of both polymers was greatly increased, causing both hole mobility and electron mobility to be more balanced. Further heating (annealing above T_m) at 300 °C led to hole and electron mobilities of the PTVPhI-C12 device being further increased; those of the PTVPhI-Eh device decreased upon heating above 250 °C. Pristine PTVPhI-Eh devices showed values of 0.18 cm^2 V^{-1} s^{-1} for hole mobility and 0.004 cm^2 V^{-1} s^{-1} for electron mobility. The hole and electron mobilities significantly improved on thermal annealing at 200 °C for 30 min, and hole and electron mobilities of 0.75 and 0.03 cm^2 V^{-1} s^{-1}, respectively, were achieved. When the annealing temperature was increased to 250 °C, the hole mobility decreased from 0.75 to 0.4 cm^2 V^{-1} s^{-1}, whereas the electron mobility was increased from 0.03 to 0.06 cm^2 V^{-1} s^{-1}. When the heating temperature

dx.doi.org/10.1021/cm303908f | Chem. Mater. XXXX, XXX, XXX−XXX

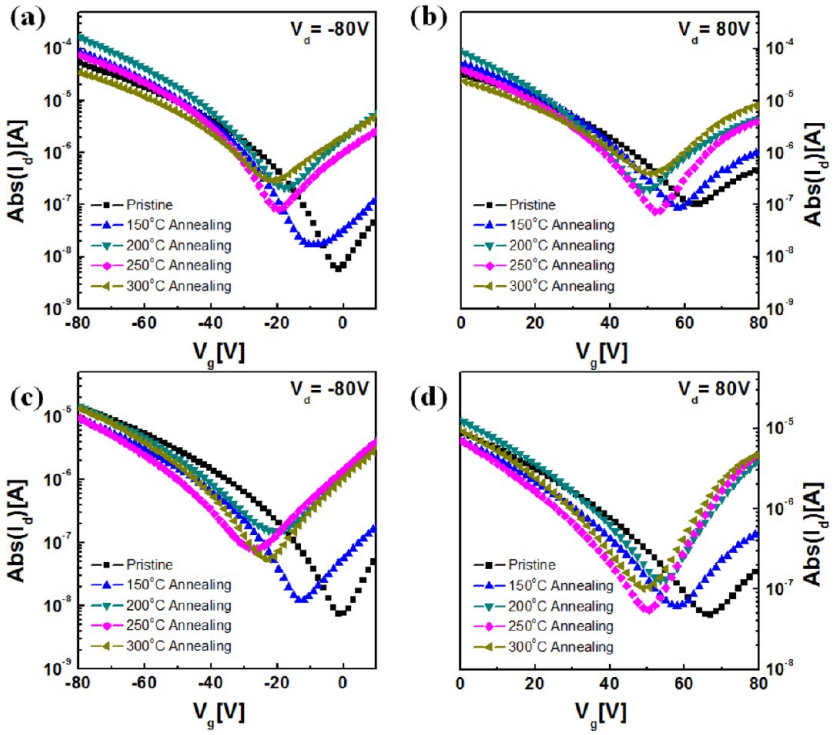

Figure 4. Ambipolar transfer characteristics in the p-channel operation mode [(a) PTVPhI-Eh and (c) PTVPhI-C12] and n-channel operation mode [(b) PTVPhI-Eh and (d) PTVPhI-C12] at various annealing temperatures.

Table 2. Top-Gate/Bottom-Contact (TG/BC) OTFT Performance for PTVPhI-Eh and PTVPhI-C12 at Various Annealing Temperatures

PTVPhI-Eh					PTVPhI-C12				
T_a[a] (°C)	μ_{hole}[b] ($cm^2 V^{-1} s^{-1}$)	$\mu_{electron}$[b] ($cm^2 V^{-1} s^{-1}$)	$V_{th,hole}$[c] (V)	$V_{th,elec}$[c] (V)	T_a (°C)	μ_{hole}[b] ($cm^2 V^{-1} s^{-1}$)	$\mu_{electron}$[b] ($cm^2 V^{-1} s^{-1}$)	$V_{th,hole}$[c] (V)	$V_{th,elec}$[c] (V)
none	0.18 ± 0.02	0.004 ± 0.002	−36 ± 2	52 ± 3	none	0.030 ± 0.006	0.0028 ± 0.0007	−33 ± 2	56 ± 1
150	0.34 ± 0.14	0.007 ± 0.002	−41 ± 2	52 ± 2	150	0.031 ± 0.003	0.0060 ± 0.001	−36 ± 5	56 ± 3
200	0.75 ± 0.18	0.03 ± 0.011	−45 ± 1	48 ± 3	200	0.047 ± 0.012	0.0443 ± 0.004	−40 ± 1	55 ± 5
250	0.4 ± 0.10	0.06 ± 0.023	−40 ± 2	53 ± 2	250	0.041 ± 0.011	0.0493 ± 0.0005	−43 ± 2	56 ± 0.8
300	0.09 ± 0.02	0.04 ± 0.018	−36 ± 2	50 ± 2	300	0.068 ± 0.022	0.0415 ± 0.005	−40 ± 1	52 ± 1

[a]Thermal annealing temperature (T_a). [b]Field effect mobilities (μ_{FET}) were averages of six to eight devices. [c]Threshold voltage (V_{th}).

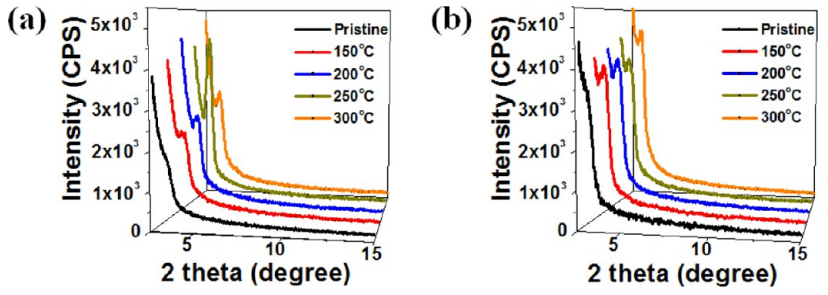

Figure 5. XRD spectra of (a) PTVPhI-Eh and (b) PTVPhI-C12 annealed at various temperatures.

was increased to 300 °C, both hole and electron mobilities were decreased. The PTVPhI-C12 devices also showed typical ambipolar characteristics but a mobility relatively lower than that of the PTVPhI-Eh devices. The pristine PTVPhI-C12 devices showed a hole mobility of 0.03 $cm^2 V^{-1} s^{-1}$ and an electron mobility of 0.0028 $cm^2 V^{-1} s^{-1}$.When the PTVPhI-C12 devices were annealed at temperatures up to 150 °C, no significant change were observed in hole and electron mobilities. However, the mobilities increased from 0.031 to 0.041 $cm^2 V^{-1} s^{-1}$ for holes and from 0.006 to 0.0493 $cm^2 V^{-1} s^{-1}$ for electrons when the annealing temperature was increased from 150 to 250 °C. As a result, PTVPhI-C12 devices exhibited well-balanced hole and electron mobilities of 0.041 and 0.0493 $cm^2 V^{-1} s^{-1}$, respectively. Unlike PTVPhI-Eh devices, the hole and electron mobilities of PTVPhI-C12 devices increased further when they were heat-treated (annealing above T_m) at 300 °C. The PTVPhI-Eh and PTVPhI-C12 devices showed little threshold voltage (V_{th}) shift for both the p- and n-

dx.doi.org/10.1021/cm303908f | Chem. Mater. XXXX, XXX, XXX−XXX

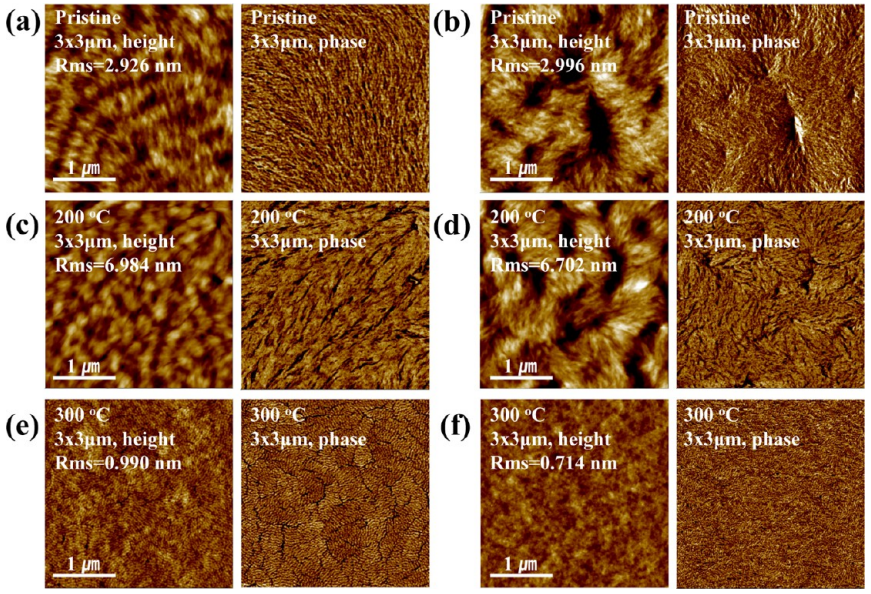

Figure 6. AFM images of pristine and annealed polymer thin films for (a, c, and e) PTVPhI-Eh and (b, d, and f) PTVPhI-C12. Images on the left and right show topographic and phase mode images, respectively.

channels via the annealing process. The details of the parameters as a function of thermal annealing temperature for both polymers are summarized in Table 2.

Microstructure and Morphologies of Polymer Thin Films and Their Correlations with Charge Transport Properties. To understand the effect of thermal annealing on the device performance of both polymers, the microstructure and surface morphology of thin films were investigated using XRD and AFM. The ordering of both polymers in thin films was investigated using XRD as shown in Figure 5. The XRD spectra of the pristine films for both polymers showed weak molecular ordering. This was because the polymer chains may not have had a sufficient amount of time to form an ordered molecular structure during the relatively fast spin-coating process.[19] After annealing had been conducted at 150 °C, distinguishable diffraction peaks were observed at 2θ values of 3.5° and 3.2° for PTVPhI-Eh and PTVPhI-C12, respectively. The intensity of the diffraction peaks in the PTVPhI-Eh film changed with an increase in the annealing temperature. The intensity of the diffraction peak gradually increased with increases in temperature of as much as 200 °C, and then a drastic increase was observed when the annealing temperature reached 250 °C. However, the intensity of these diffraction peaks decreased upon further heating (annealing above T_m) to 300 °C. The changes in diffraction peaks for the PTVPhI-Eh film were strongly correlated with electron mobility. A maximal electron mobility of 0.06 $cm^2\ V^{-1}\ s^{-1}$ was obtained at 250 °C, but hole mobility began to decrease drastically from 0.75 (200 °C) to 0.4 $cm^2\ V^{-1}\ s^{-1}$ at 250 °C. This result means that the strongest interchain ordering induces a favorable chain conformation for electron hopping transport, such as the alignment of transport sites, while strong interchain ordering does not predominantly act on hole transport. The next section provides a more detailed discussion about hole and electron charge transport. On the other hand, in the case of the PTVPhI-C12 film, there was no significant change in diffraction peaks when the annealing/heating temperature was increased from 150 to 300 °C. This means that chain reorganization is more easily achieved by thermal annealing for PTVPhI-Eh than it is for PTVPhI-C12. Both polymers showed more a diffraction peak at 300 °C clearer than those of pristine films, despite the large diminution in intensity that was observed for long wavelength absorption. As a result, electron mobility was more improved than those of pristine films due to the improvement in molecular ordering and packing. Despite the increase in the magnitude of the XRD peak by the thermal annealing process, the shift in the position of the XRD peak was negligible, which indicates no change in the $\pi-\pi$ stacking distance between intermolecules.

Figure 6 shows the topography and phase images of both polymers at various annealing temperatures. As shown in panels a and b of Figure 6, pristine film of PTVPhI-Eh and PTVPhI-C12 showed clustered nanofibrillar structures. Similar morphological changes in both thin films were observed when the films were annealed at 200 °C. The widths and domain sizes of clustered nanofibers were further increased compared with those of the pristine samples. The surface roughness of PTVPhI-Eh and PTVPhI-C12 significantly increased from 2.9 to 6.9 nm and from 2.9 to 6.7 nm, respectively. It is worth noting that well-defined domains and clustered nanofibers are favorable to the facilitation of domain interconnectivity, and, thus, provide an efficient pathway for charge transport. However, heating (annealing above T_m) films of both polymers at 300 °C showed a different surface morphology. The PTVPhI-Eh film showed disconnected nanorod-like structures rather than clustered nanofibillar structures. In addition, surface defects were formed after the film was annealed above the T_m of the polymers (see Figure 7). These disconnected nanorod-like structures and surface defects interrupted the charge transport pathway and resulted in an increased level of charge trapping. By contrast, the surface morphology of the PTVPhI-C12 film at 300 °C showed the presence of nanofibrillar structures, similar to reports of other semicrystalline polymers such as rr-P3HT. These morphological dependencies on the annealing temperature were in good agreement with ambipolar mobility changes.

Correlation between Intra- and Interchain Conformation and Charge Transport Properties with the

dx.doi.org/10.1021/cm303908f | Chem. Mater. XXXX, XXX, XXX−XXX

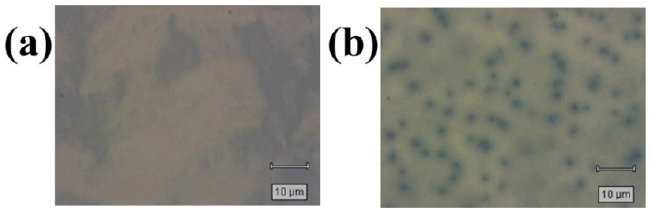

Figure 7. Optical microscope images of (a) pristine and (b) 300 °C annealed PTVPhI-Eh thin films.

Annealing Process. The mechanisms of hole and electron transport were studied using the electron-state density distribution, Raman spectroscopy, and XRD. First, quantum chemical calculations (ZINDO/S excited-state energy calculations on AM1 optimized geometries) were conducted for the electron-state density distribution of the HOMO and LUMO of the structurally optimized PTVPhI dimer and trimer to explain the presence of ambipolarity in a PTVPhI backbone (Figure 8). The side chains in a PTVPhI backbone were excluded in this model because the alkyl chains have little or no impact on the backbone conformation and the charge density isosurface.[12]

In the typical D−A polymer, F8BT, it is known that the HOMO level is fully delocalized along the polymer backbone and that the LUMO is strongly localized on the electron-accepting unit of the polymer backbone.[12b] Therefore, hole transport is expected to move efficiently along the polymer backbone, while electron transport is limited. The localized LUMO on the electron-accepting unit can obstruct intra- and interchain charge transport, and for this reason, good alignment or ordering of the localized LUMO is required. However, as shown in Figure 8, the PTVPhI backbone shows that the charge densities of HOMO and LUMO are delocalized across the polymer backbone, even though the LUMO appears to be less delocalized across the backbone than the HOMO. The intrachain hole and electron transport are thus efficient along the conjugated polymer backbone within an effective conjugation length, particularly when the polymer chains are well aligned in the transport direction and when there is an absence of chemical defects. This result is consistent with the results of Raman spectroscopy and XRD. From the Raman analysis, either the planarity or the level of conjugation of the PTVPhI backbone was increased with the annealing process, compared with that of the solution and pristine film. Increasing the backbone planarity or level of conjugation could help with intrachain hole and electron transport and lead to improvements in the hole and electron mobilities of the polymer. In addition, XRD spectra showed improvement of interchain ordering by thermal annealing, and thus, an increase in the extent of interchain hole and electron transport could be observed. In particular, electron mobility showed a significant improvement compared with that of hole mobility. Typically, the main charge transfer route within the ordered domains is an intrachain rather than an interchain one if the charge densities of both HOMO and LUMO are well-delocalized over the polymer backbone. However, intrachain electron transport of these polymers is relatively limited and not expected to be a very efficient transport compared to hole transport, because the LUMO is less delocalized along the backbone than the HOMO, as shown in Figure 8. Therefore, it would be necessary to create another transport pathway for electrons to make up for limited intrachain transport, and an increased interchain ordering by annealing process could efficiently create another transport pathway. For that reason, electron mobility is strongly affected and more improved by interchain ordering. By contrast, the effect was relatively small in hole transport because intrachain hole transport is significantly predominant over interchain hopping when the HOMO is strong delocalized over the conjugated backbone without strong fluctuations in the torsion angles between adjacent units.[20]

However, although the planarity and ordering of PTVPhI polymers were improved by thermal annealing, the hole and electron mobilities were not perfectly balanced. This effect can be attributed to the energy level mismatch for hole and electron injection between the polymer frontier molecular orbital and the Au electrode. The difference in charge injection properties can be corrected by the insertion of an interlayer between an injection electrode and a conjugated polymer.[7a] Figure 9 shows the schematic illustration of a PTVPhI polymer chain conformation and hole and electron transport in a pristine and thermally annealed film. Figure 9a is an illustration of weak polymer chain ordering in pristine films, as observed in the XRD and Raman data. Annealed polymer chains can reorganize themselves in a more planar and ordered conformation of intra- and interchains (Figure 9b). The reorganization of polymer

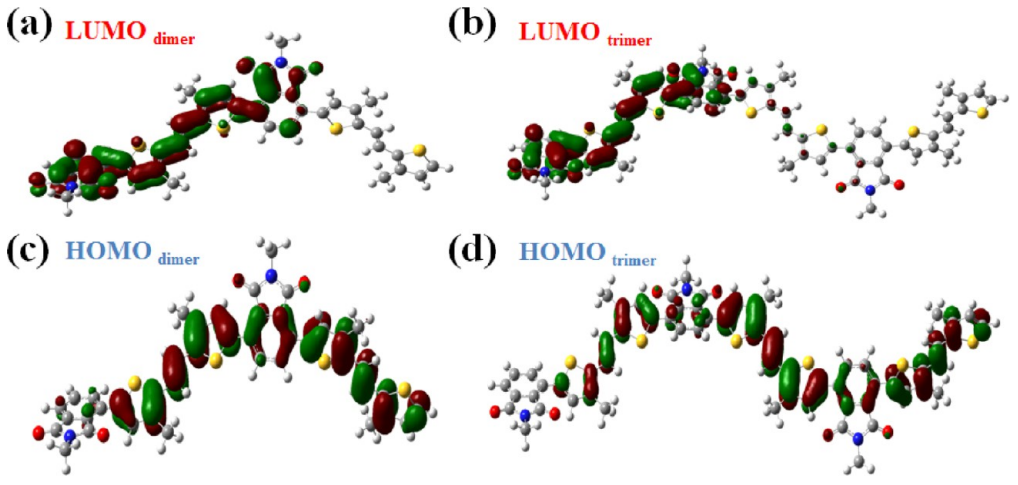

Figure 8. Electron-state density distribution of the HOMO and LUMO in the structure-optimized dimer (a and c) and trimer (b and d), respectively.

dx.doi.org/10.1021/cm303908f | *Chem. Mater.* XXXX, XXX, XXX−XXX

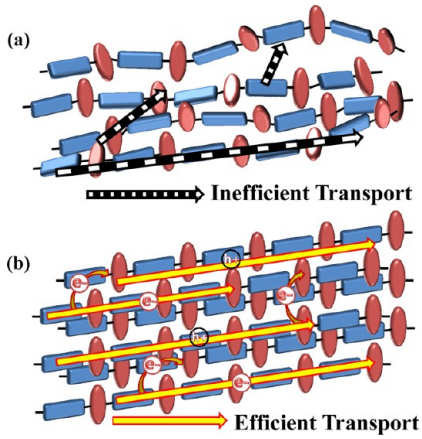

Figure 9. Schematic illustration of the change in polymer chain conformation by the annealing process: (a) nonannealed polymer film and (b) annealed polymer film.

chains induces more efficient intra- and interchain charge transport, resulting in increased hole and electron mobilities.

Characterization of a Complementary Inverter. We demonstrated complementary-like ambipolar inverters using a PTVPhI-Eh polymer. PTVPhI-Eh inverters consist of two identical TG/BC OTFTs that are connected. They were fabricated by spin-coating without a patterning process for the conjugated polymer. Figure 10 shows the voltage transfer characteristics (VTCs) and output voltage gains of a PTVPhI-Eh ambipolar inverter at a supplied voltage (V_{DD}) of ±60 V after annealing at various temperatures. As shown in Figure 10a, PTVPhI-Eh ambipolar inverters showed typical Z-shaped-like VTCs due to the noise of the pull-down transistor at a zero gate bias. The inverting voltage of a PTVPhI-Eh inverter without annealing was largely shifted in the positive direction from an ideal value (half of V_{DD}). This asymmetry of VTCs in the pristine CMOS inverter resulted in the unbalanced characteristics (μ_{FET} and V_{th}) of pull-up and pull-down transistors.[21] The largely shifted inverting voltages were greatly improved for thermally annealed devices because of the more balanced hole and electron mobilities. Panels c and d of Figure 10 show the VTCs and output voltage gains, respectively, for various supply voltages at 250 °C of an annealed PTVPhI-Eh ambipolar inverter. The sharp switching curve of PTVPhI-Eh inverters exhibited a maximal voltage gain of ~40 at V_{DD} = 70 V. In addition, the inverting voltage and hysteresis of PTVPhI-C12 inverters showed trends similar to those of PTVPhI-Eh inverters, as shown in Figure S6 of the Supporting Information.

4. CONCLUSIONS

We have synthesized and characterized a series of D−A copolymers (PTVPhI-Eh and PTVPhI-C12) based on a dodecyl-TV unit and an alkyl-substituted phthalimide unit. These polymers showed energy levels that are suitable for application in ambipolar OTFTs, and consequently, they showed good ambipolar mobility. The maximal hole and electron mobilities of both polymers were measured: for PTVPhI-Eh, μ_h = 0.75 cm^2 V^{-1} s^{-1} and μ_e = 0.06 cm^2 V^{-1} s^{-1}; for PTVPhI-C12, μ_h = 0.068 cm^2 V^{-1} s^{-1} and μ_e = 0.049 cm^2 V^{-1} s^{-1}. Our studies of the charge transport of PTVPhI polymers upon thermal annealing have demonstrated that

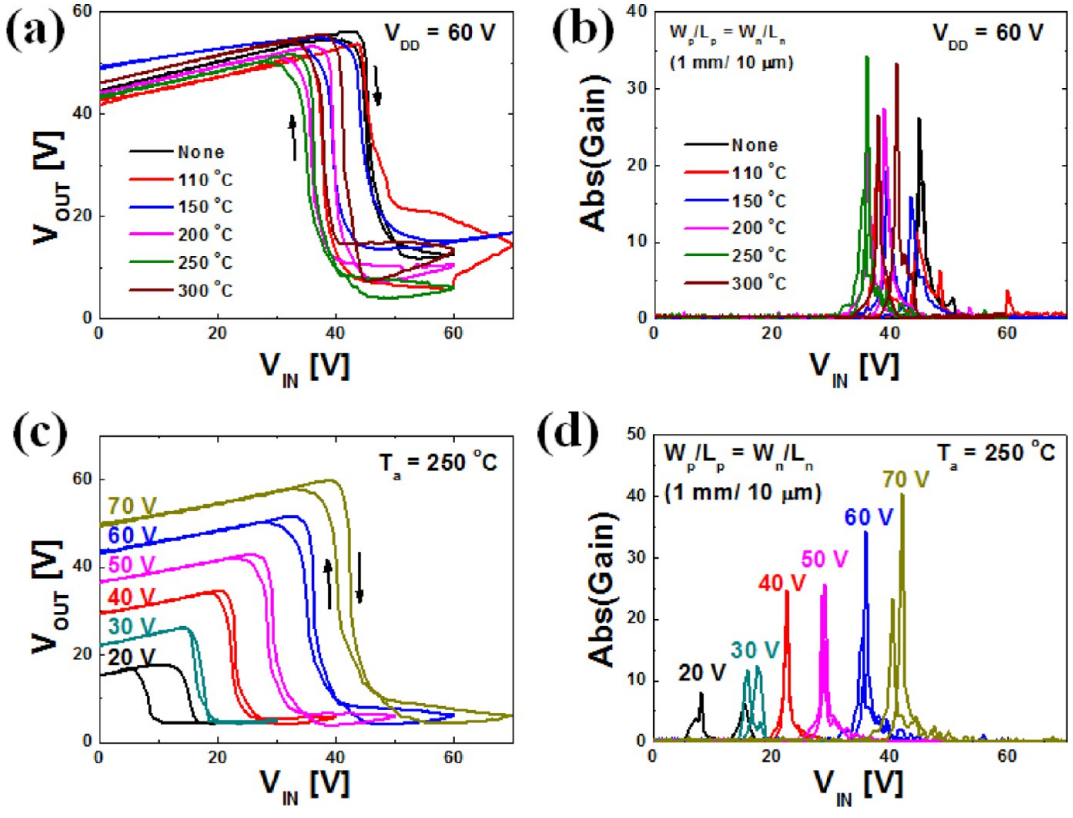

Figure 10. (a) Voltage transfer characteristics (VTCs) and (b) output voltage gains of complementary inverters based on a PTVPhI-Eh transistor after annealing at various temperatures. (c) VTCs and (d) output voltage gains of complementary inverters based on a PTVPhI-Eh transistor (annealed at 250 °C) for various supplied voltages.

dx.doi.org/10.1021/cm303908f | Chem. Mater. XXXX, XXX, XXX−XXX

changes in intra- and interchain conformation and packing affect both hole and electron mobilities. The pristine films of both polymers showed lower hole and electron mobilities as a result of an inefficient charge transport pathway due to a disordered conformation. Upon thermal annealing, increasing the backbone planarity or level of conjugation could help with intrachain hole and electron transport and lead to improvements in the hole and electron mobilities of the polymer. However, intrachain electron transport is relatively limited compared to hole transport because the LUMO is less delocalized along the backbone than the HOMO. Therefore, after annealing had been conducted, electron transport is more affected by interchain ordering, and that makes another pathway for efficient electron transport to neighboring chains, resulting in increased electron mobility. On the other hand, intrachain hole transport is significantly predominant over interchain hopping because the HOMO is strongly delocalized over the backbone and consequently hole transport is less affected by interchain ordering. Finally, we demonstrated complementary-like ambipolar inverters using a PTVPhI-Eh polymer. After annealing had been conducted at 250 °C, the PTVPhI-Eh inverter showed improvement in inverting voltage that is close to $0.5V_{DD}$ and a sharp switching signal and a large gain of ∼40 due to a better balance for hole and electron mobility.

■ ASSOCIATED CONTENT

Supporting Information

Thermal properties, cyclic voltammograms, XRD, and device characterization. This material is available free of charge via the Internet at http://pubs.acs.org.

■ AUTHOR INFORMATION

Corresponding Author

*E-mail: kimdy@gist.ac.kr (D.-Y.K.) or yynoh@dongguk.edu (Y.-Y.N.).

Notes

The authors declare no competing financial interest.

■ ACKNOWLEDGMENTS

This work was financially supported by a National Research Foundation of Korea (NRF) grant funded by the Korea government (MEST) (Grant 2012-0008723) and the Dongguk University Fund of 2013. We thank the Korea Basic Science Institute (KBSI) and National Center for Inter-University Research Facilities (NCIRF, Seoul National University) for AFM and EA measurements.

■ REFERENCES

(1) (a) Facchetti, A. *Chem. Mater.* **2011**, *23*, 733. (b) Beaujuge, P. M.; Frechet, J. M. J. *J. Am. Chem. Soc.* **2011**, *133*, 20009. (c) Forrest, S. R. *Nature* **2004**, *428*, 911. (d) Sun, J.; Zhang, B.; Katz, H. E. *Adv. Funct. Mater.* **2011**, *21*, 29. (e) Yang, Y.; Wudl, F. *Adv. Mater.* **2009**, *21*, 1401. (f) Wang, S.; Kiersnowski, A.; Pisula, W.; Mullen, K. *J. Am. Chem. Soc.* **2012**, *134*, 4015.

(2) (a) Baeg, K. J.; Khim, D.; Kim, D. Y.; Jung, S. W.; Koo, J. B.; You, I. K.; Yan, H.; Facchetti, A.; Noh, Y. Y. *J. Polym. Sci., Part B: Polym. Phys.* **2011**, *49*, 62. (b) Fukuda, H.; Ise, M.; Kogure, T.; Takano, N. *Thin Solid Films* **2004**, *464*, 441. (c) Tremblay, N. J.; Jung, B. J.; Breysse, P.; Katz, H. E. *Adv. Funct. Mater.* **2011**, *21*, 4314. (d) Heremans, P.; Gelinck, G. H.; Muller, R.; Baeg, K. J.; Kim, D. Y.; Noh, Y. Y. *Chem. Mater.* **2011**, *23*, 341.

(3) (a) Kim, J.; Lim, B.; Baeg, K. J.; Noh, Y. Y.; Khim, D.; Jeong, H. G.; Yun, J. M.; Kim, D. Y. *Chem. Mater.* **2011**, *23*, 4663. (b) McCulloch, I.; Heeney, M.; Bailey, C.; Genevicius, K.; Macdonald, I.; Shkunov, M.; Sparrowe, D.; Tierney, S.; Wagner, R.; Zhang, W. M.; Chabinyc, M. L.; Kline, R. J.; McGehee, M. D.; Toney, M. F. *Nat. Mater.* **2006**, *5*, 328. (c) Yan, H.; Chen, Z. H.; Zheng, Y.; Newman, C.; Quinn, J. R.; Dotz, F.; Kastler, M.; Facchetti, A. *Nature* **2009**, *457*, 679. (d) Tsao, H. N.; Cho, D. M.; Park, I.; Hansen, M. R.; Mavrinskiy, A.; Yoon, D. Y.; Graf, R.; Pisula, W.; Spiess, H. W.; Mullen, K. *J. Am. Chem. Soc.* **2011**, *133*, 2605.

(4) (a) Bijleveld, J. C.; Zoombelt, A. P.; Mathijssen, S. G. J.; Wienk, M. M.; Turbiez, M.; de Leeuw, D. M.; Janssen, R. A. J. *J. Am. Chem. Soc.* **2009**, *131*, 16616. (b) Mohebbi, A. R.; Yuen, J.; Fan, J.; Munoz, C.; Wang, M. F.; Shirazi, R. S.; Seifter, J.; Wudl, F. *Adv. Mater.* **2011**, *23*, 4644. (c) Kim, F. S.; Guo, X. G.; Watson, M. D.; Jenekhe, S. A. *Adv. Mater.* **2010**, *22*, 478. (d) Yuen, J. D.; Kumar, R.; Zakhidov, D.; Seifter, J.; Lim, B.; Heeger, A. J.; Wudl, F. *Adv. Mater.* **2011**, *23*, 3780. (e) Cho, S.; Lee, J.; Tong, M.; Seo, J. H.; Yang, C. *Adv. Funct. Mater.* **2011**, *21*, 1910. (f) Lee, J.; Han, A.-R.; Hong, J.; Seo, J. H.; Oh, J. H.; Yang, C. *Adv. Funct. Mater.* **2012**, *22*, 4128.

(5) (a) Chu, T. Y.; Lu, J. P.; Beaupre, S.; Zhang, Y. G.; Pouliot, J. R.; Wakim, S.; Zhou, J. Y.; Leclerc, M.; Li, Z.; Ding, J. F.; Tao, Y. *J. Am. Chem. Soc.* **2011**, *133*, 4250. (b) Sonar, P.; Singh, S. P.; Li, Y. N.; Ooi, Z. E.; Ha, T. J.; Wong, I.; Soh, M. S.; Dodabalapur, A. *Energy Environ. Sci.* **2011**, *4*, 2288. (c) Qu, S. Y.; Tian, H. *Chem. Commun.* **2012**, *48*, 3039. (d) Bronstein, H.; Chen, Z. Y.; Ashraf, R. S.; Zhang, W. M.; Du, J. P.; Durrant, J. R.; Tuladhar, P. S.; Song, K.; Watkins, S. E.; Geerts, Y.; Wienk, M. M.; Janssen, R. A. J.; Anthopoulos, T.; Sirringhaus, H.; Heeney, M.; McCulloch, I. *J. Am. Chem. Soc.* **2011**, *133*, 3272. (e) Ashraf, R. S.; Chen, Z. Y.; Leem, D. S.; Bronstein, H.; Zhang, W. M.; Schroeder, B.; Geerts, Y.; Smith, J.; Watkins, S.; Anthopoulos, T. D.; Sirringhaus, H.; de Mello, J. C.; Heeney, M.; McCulloch, I. *Chem. Mater.* **2011**, *23*, 768. (f) Amb, C. M.; Chen, S.; Graham, K. R.; Subbiah, J.; Small, C. E.; So, F.; Reynolds, J. R. *J. Am. Chem. Soc.* **2011**, *133*, 10062.

(6) (a) Sonar, P.; Singh, S. P.; Li, Y.; Soh, M. S.; Dodabalapur, A. *Adv. Mater.* **2010**, *22*, 5409. (b) Li, Y.; Singh, S. P.; Sonar, P. *Adv. Mater.* **2010**, *22*, 4862.

(7) (a) Baeg, K. J.; Kim, J.; Khim, D.; Caironi, M.; Kim, D. Y.; You, I. K.; Quinn, J. R.; Facchetti, A.; Noh, Y. Y. *ACS Appl. Mater. Interfaces* **2011**, *3*, 3205. (b) Chen, Z. Y.; Lemke, H.; Albert-Seifried, S.; Caironi, M.; Nielsen, M. M.; Heeney, M.; Zhang, W. M.; McCulloch, I.; Sirringhaus, H. *Adv. Mater.* **2010**, *22*, 2371. (c) Natali, D.; Caironi, M. *Adv. Mater.* **2012**, *24*, 1357. (d) Chen, Z. Y.; Lee, M. J.; Ashraf, R. S.; Gu, Y.; Albert, S.; Nielsen, M. M.; Schroeder, B.; Anthopoulos, T. D.; Heeney, M.; McCulloch, I.; Sirringhaus, H. *Adv. Mater.* **2012**, *24*, 647.

(8) (a) Goldoni, F.; Janssen, R. A. J.; Meijer, E. W. *J. Polym. Sci., Part A: Polym. Chem.* **1999**, *37*, 4629. (b) Roncali, J. *Macromol. Rapid Commun.* **2007**, *28*, 1761. (c) Fu, Y.; Cheng, H.; Elsenbaumer, R. L. *Chem. Mater.* **1997**, *9*, 1720. (d) Elandaloussi, E. H.; Frère, P.; Richomme, P.; Orduna, J.; Garin, J.; Roncali, J. *J. Am. Chem. Soc.* **1997**, *119*, 10774. (e) Jestin, I.; Frere, P.; Mer-cier, N.; Levillain, E.; Stievenard, D.; Roncali, J. *J. Am. Chem. Soc.* **1998**, *120*, 8150. (f) Jeeva, S.; Lukoyanova, O.; Karas, A.; Davand, A.; Rosei, F.; Perepichka, D. F. *Adv. Funct. Mater.* **2010**, *20*, 1661.

(9) (a) Guo, X. G.; Watson, M. D. *Org. Lett.* **2008**, *10*, 5333. (b) Liu, C. A.; Liu, Z. H.; Lemke, H. T.; Tsao, H. N.; Naber, R. C. G.; Li, Y.; Banger, K.; Mullen, K.; Nielsen, M. M.; Sirringhaus, H. *Chem. Mater.* **2010**, *22*, 2120. (c) Guo, X. G.; Ortiz, R. P.; Zheng, Y.; Hu, Y.; Noh, Y. Y.; Baeg, K. J.; Facchetti, A.; Marks, T. J. *J. Am. Chem. Soc.* **2011**, *133*, 1405.

(10) Guo, X. G.; Kim, F. S.; Jenekhe, S. A.; Watson, M. D. *J. Am. Chem. Soc.* **2009**, *131*, 7206.

(11) Oton, F.; Pfattner, R.; Pavlica, E.; Olivier, Y.; Moreno, E.; Puigdollers, J.; Bratina, G.; Cornil, J.; Fontrodona, X.; Mas-Torrent, M.; Veciana, J.; Rovira, C. *Chem. Mater.* **2011**, *23*, 851.

(12) (a) Cho, S.; Seo, J. H.; Kim, S. H.; Song, S.; Jin, Y.; Lee, K.; Suh, H.; Heeger, A. *J. Appl. Phys. Lett.* **2008**, 93. (b) Donley, C. L.; Zaumseil, J.; Andreasen, J. W.; Nielsen, M. M.; Sirringhaus, H.; Friend, R. H.; Kim, J. S. *J. Am. Chem. Soc.* **2005**, *127*, 12890. (c) Cornil, J.; Gueli, I.; Dkhissi, A.; Sancho-Garcia, J. C.; Hennebicq, E.; Calbert, J.

P.; Lemaur, V.; Beljonne, D.; Bredas, J. L. *J. Chem. Phys.* **2003**, *118*, 6615. (d) Vooren, A. V.; Kim, J. S.; Cornil, J. *ChemPhysChem* **2008**, *9*, 989.
(13) Lee, C.; Yang, W.; Parr, R. G. *Phys. Rev. B* **1988**, *37*, 785.
(14) Irikura, K. K.; Johnson, R. D.; Kacker, R. N. *J. Phys. Chem. A* **2005**, *109*, 8430.
(15) (a) Ridley, J.; Zerner, M. *Theor. Chem. Acc.* **1973**, *32*, 111. (b) Huang, Y.-S.; Westenhoff, S.; Avilov, I.; Sreearunothai, P.; Hodgkiss, J. M.; Deleener, C.; Friend, R. H.; Beljonne, D. *Nat. Mater.* **2008**, *7*, 483.
(16) Mondal, R.; Becerril, H. A.; Verploegen, E.; Kim, D.; Norton, J. E.; Ko, S.; Miyaki, N.; Lee, S.; Toney, M. F.; Bredas, J. L.; McGehee, M. D.; Bao, Z. N. *J. Mater. Chem.* **2010**, *20*, 5823.
(17) (a) Hernandez, V.; Castiglioni, C.; Del Zoppo, M.; Zerbi, G. *Phys. Rev. B* **1994**, *50*, 9815. (b) Tsoi, W. C.; James, D. T.; Kim, J. S.; Nicholson, P. G.; Murphy, C. E.; Bradley, D. D. C.; Nelson, J.; Kim, J.-S. *J. Am. Chem. Soc.* **2011**, *133*, 9834.
(18) McCulloch, I.; Heeney, M.; Chabinyc, M. L.; DeLongchamp, D.; Kline, R. J.; Coelle, M.; Duffy, W.; Fischer, D.; Gundlach, D.; Hamadani, B.; Hamilton, R.; Richter, L.; Salleo, A.; Shkunov, M.; Sporrowe, D.; Tierney, S.; Zhong, W. *Adv. Mater.* **2009**, *21*, 1091.
(19) Skompska, M. *Synth. Met.* **2010**, *160*, 1.
(20) (a) Lan, Y.-K.; Yang, C. H.; Yang, H.-C. *Polym. Int.* **2010**, *59*, 16. (b) Vooren, A. V.; Kim, J.-S.; Cornil, J. *ChemPhysChem* **2008**, *9*, 989.
(21) Wu, P. T.; Kim, F. S.; Jenekhe, S. A. *Chem. Mater.* **2011**, *23*, 4618.